

Random motion of a circle microswimmer in a random environment

Oleksandr Chepizhko & Thomas Franosch

Institut für Theoretische Physik, Universität Innsbruck, Technikerstraße 21A, A-6020 Innsbruck, Austria.

E-mail: oleksandr.chepizhko@uibk.ac.at

May 2020

Abstract. We simulate the dynamics of a single circle microswimmer exploring a disordered array of fixed obstacles. The interplay of two different types of randomness, quenched disorder and stochastic noise, is investigated to unravel their impact on the transport properties. We compute lines of isodiffusivity as a function of the rotational diffusion coefficient and the obstacle density. We find that increasing noise or disorder tends to amplify diffusion, yet for large randomness the competition leads to a strong suppression of transport. We rationalize both the suppression and amplification of transport by comparing the relevant time scales of the free motion to the mean period between collisions with obstacles.

1. Introduction

Transport properties of active particles [1, 2] change significantly when they are exposed to a strongly heterogeneous medium [3, 4]. Both amplification [5, 6, 7] and suppression of diffusion [8, 9, 10, 11, 12] with an increase of introduced obstacle density has been found in various scenarios, in experiments and in computer simulations. For active particles, not only is diffusion affected, but ratchet effects [4], negative differential mobility [13, 14, 15], and clogging [16] emerge. Similar peculiar behavior has been seen for active Janus particles in visco-elastic media, which has been rationalized in terms of retarded torques coupling back to the propulsion force [17, 18], or for active particles exposed to external fields as in gravitaxis [19] and chemotaxis [20, 21].

When these active particles undergo scattering from the inhomogeneities in the environment, diffusion is usually suppressed [9, 7, 22]. Yet, transport may be also enhanced, particularly, for circle microswimmers [23]. In general, active particles can interact with their surroundings in complex ways, for example, the microswimmers can follow the boundaries of obstacles, sometimes for particularly long times [24, 25, 26, 27, 28], which can be rationalized using hydrodynamic theories [29, 30, 31, 32]. On one hand, the boundary-following mechanism can slow diffusion [27, 11], if the particles are trapped for long times around heterogeneities. On the other hand, there

is theoretical [33], numerical [34, 6, 7], and experimental [5, 35] evidence that adding obstacles can, under certain conditions, speed up transport. For example, diffusion is amplified if the microswimmers are scattered forward [7], or simply allowed to propagate along connected obstacles [6]. Yet, in more general cases the properties that define the distinction between enhancement and hindrance of transport still need to be investigated.

Up to now a significant number of theoretical and experimental studies have used non-overlapping obstacles or pillars placed on a regular lattice [27, 28, 36, 7, 22], while only few studies [9, 10, 11] focused on random environments. Typically, a probe particle has been chosen to be a straight-swimming active Brownian particle [8, 9], or a particle undergoing run-and-tumble dynamics [37, 33]. To extend our understanding of transport properties of real systems, both these constraints should be relaxed. The paradigmatic Lorentz model [38, 39, 40] constitutes a reference system to study how transport properties of probe particles in heterogeneous media depend on the microscopic motion of the particles and their environment [41, 42, 43, 44]. The main feature of the Lorentz model is that the obstacles are placed randomly and can overlap. Regarding the model of an active particle, a Brownian *circle* swimmer can be considered as a more realistic approach than those used previously, as, in general, microswimmers will not move in straight lines even for short times. Rather, the trajectories will be intrinsically curved, due to asymmetries in shape or the propulsion mechanism [45, 46], or hydrodynamic coupling to walls [29, 47]. If the angular drift is large compared to the rotational diffusion, many circles are completed before the orientation is randomized [48, 49]. Currently, a complete study of transport amplification and suppression which includes both circular motion subject to noise and the wall-following mechanism, in a randomly distributed array of obstacles, is lacking.

Here, we investigate the dynamics of a realistic model for a circle microswimmer in a disordered environment. We start by adding rotational diffusion to the motion of an ideal active circle swimmer [6]. We show that a small angular noise slightly amplifies diffusion relative to an ideal microswimmer and leaves the dependence on its orbit radius almost untouched. For high values of noise the diffusivity becomes independent of the orbit radius and is determined solely by the obstacle density. Then, we construct isodiffusivity contours in the non-equilibrium state diagram spanned by the density of obstacles and the rotational diffusion coefficient. We show that small amounts of both kinds of randomness amplify diffusion, while their interplay at large values leads to a suppression of transport. The position of the boundary between regions of enhanced and hindered diffusion strongly depends on the orbit radius. We explain the differences in the transport by exploring the short-time behavior of the mean-squared displacement of a free noisy microswimmer.

2. Model and methods

We consider a circle microswimmer meandering in a disordered array of disk-like obstacles in a plane. In free space the microswimmer moves with fixed propulsion speed v_0 along its instantaneous orientation, parameterized in terms of a time-dependent angle $\theta(t)$. Then, the particle moves with velocity

$$\frac{d}{dt}\vec{r}(t) = v_0(\cos \theta(t), \sin \theta(t))^T. \quad (1)$$

The orientation itself changes in time by an angular drift Ω as well as by rotational diffusion [48, 45, 49]

$$\frac{d}{dt}\theta(t) = \Omega + \sqrt{2D_\theta}\xi(t). \quad (2)$$

The direction of motion experiences a constant drift $\Omega = v_0/R > 0$ (particle moves counterclockwise), where R is referred to as the orbit radius, and the orientational dynamics is subject to Gaussian white noise $\xi(t)$, characterized by $\langle \xi(t) \rangle = 0$, $\langle \xi(t)\xi(t') \rangle = \delta(t-t')$ with rotational diffusion coefficient $D_\theta > 0$. In principle, one could add to Eq. (1) also translational noise with short-time diffusion coefficient D_{trans} . Yet, for microswimmers active propulsion typically dominates translational diffusion (except at short times) therefore we set $D_{\text{trans}} = 0$ in the following, in line with other works on active Brownian particles [3, 50], to focus on the transport properties purely caused by an interplay of rotational diffusion with quenched disorder. We integrate the equations of motion by means of event-driven (pseudo-) Brownian dynamics simulations [51].

We refer to our particle as a “microswimmer” since the interaction with the obstacles is hydrodynamic in nature, not steric, as it usually is for active Brownian particles. However, we will model this interaction with a simplified rule. The microswimmer interacts with obstacles *via* a boundary-following mechanism recently introduced [6]. Upon hitting an obstacle at a polar angle φ_i (relative to the center of the obstacle) the microswimmer starts to follow its boundary [6], see Fig. 1. The orientation of the swimmer θ remains fixed during this interaction process. A random number $\Delta \in [-0.9\pi/2, 0.9\pi/2]$ is drawn and the escape position on the boundary φ_e is computed as follows,

$$\varphi_e = (\theta - \Delta) \bmod 2\pi. \quad (3)$$

The escape position φ_e does not depend explicitly on the collision position φ_i . The choice of the interval for Δ assures that the direction of motion θ will point outside of the obstacle when the microswimmer reaches the position φ_e . If the microswimmer cannot reach this position because it hits another obstacle first (i.e. when an intersection with the next obstacle is at φ_o , $\varphi_i < \varphi_o < \varphi_e$), a new random number is drawn and the process continues until the microswimmer escapes from the surface of the connected cluster of obstacles. We illustrate the interaction in Fig. 1.

The rules have been chosen to fulfill the following constraints. The random angle Δ should not come too close to $\pm\pi/2$ since this leads to numerical artifacts, the particles

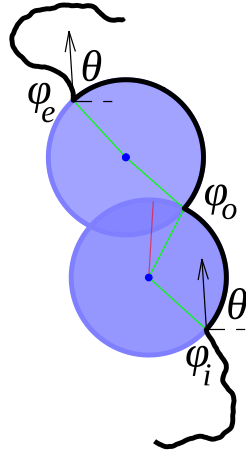


Figure 1. Illustration of the particle interaction with obstacles. The particle moves from bottom to top. The trajectory of the particle is shown as solid black line. The obstacles are shown as blue circles. The particle's orientation θ remains unchanged throughout its motion along the obstacle boundaries. The position of the collision on the first obstacle is denoted as φ_i , φ_o is the position of the intersection of obstacles, φ_e refers to the escape position on the second obstacle. The angles φ are measured with respect to the corresponding obstacle. Green lines are radii connecting centers of obstacles with corresponding particle positions. The red line denotes the escape position that was not possible to reach because of obstacle overlap. In the given example a particle collides with an obstacle at the point characterized by the angle φ_i . Then a random number is drawn and a new escape position is calculated as shown by the red line. Yet, the position is not reachable as the obstacles overlap. Thus, the particle moves to the position of obstacle intersection, φ_o . Next, a new random number is drawn and a new escape position φ_e is computed. As the position is not inside another obstacle the particle leaves the surface into accessible space.

get trapped and many recollisions may occur. We choose the particle's orientation θ to be constant while sliding along the obstacle, rather than evolving according to some noisy dynamics, in order to have a closer connection to the previous idealized model [6]. Also, this rule simplifies the numerical simulations while being sufficiently close to real systems.

The environment consists of randomly and independently placed obstacles of size $\sigma > 0$, which serves as the unit of length. Similarly σv_0^{-1} sets the unit of time. Then, the structural properties of the obstacle configuration are characterized solely by the reduced density

$$n^* := \frac{N\sigma^2}{L^2}, \quad (4)$$

a dimensionless parameter, with N being the number of obstacles and L the linear system size. The free motion can be characterized by another dimensionless parameter, referred to as the quality factor

$$M := \frac{\Omega}{2\pi D_\theta} = \frac{v_0}{2\pi R D_\theta}. \quad (5)$$

Then M is a measure of how many circles a microswimmer can complete before the orientation becomes randomized in diffusion time $1/D_\theta$ [48, 49].

In our system, long-range transport prevails at any obstacle density smaller than the critical one $n_c^* = 0.359081\dots$ [52] where the localization transition occurs. To characterize the transport properties of the system at densities $n^* < n_c^*$ we have measured the mean-squared displacement

$$\delta r^2(t) := \left\langle [\vec{R}(t) - \vec{R}(0)]^2 \right\rangle, \quad (6)$$

where $\vec{R}(t)$ denotes the position of the swimmer at time t . At long times the mean-squared displacement is expected to be proportional to time

$$\delta r^2(t) \simeq 4Dt, \quad t \rightarrow \infty, \quad (7)$$

with the diffusion coefficient (diffusivity) D . In our data analysis we extract the diffusivity by the limit

$$D = \lim_{t \rightarrow \infty} \frac{1}{4} \frac{d}{dt} \delta r^2(t). \quad (8)$$

In the absence of obstacles the long-time diffusion coefficient can be calculated analytically [48, 49, 53]

$$D = D(R, D_\theta, n^* = 0) = \frac{v_0^2 D_\theta}{2(D_\theta^2 + v_0^2/R^2)}. \quad (9)$$

One infers that for each value of R there is an optimal rotational diffusion coefficient D_θ^{opt} maximizing transport in the obstacle-free system:

$$D_\theta^{\text{opt}} := \frac{v_0}{R} = \Omega. \quad (10)$$

Together with the definition from Eq. (5) we obtain the universal value of the quality factor that maximizes diffusion, $M^{\text{opt}} := 1/2\pi$.

Our reference system will be the ideal circle microswimmer ($D_\theta = 0$) in a crowded environment. There the state diagram consists of three regions [6] separated by sharp boundaries. Essentially, it is the same as the corresponding state diagram of the magneto-transport problem [54, 55] for electrons moving in a constant perpendicular magnetic field and interacting with obstacles via *specular scattering*. At low obstacle densities an *orbiting* state emerges. Here the orbit radius is not large enough for a microswimmer to reach one obstacle cluster from another, such that the microswimmers are simply localized around a finite number of obstacles, and so there is no diffusion. Upon increasing the density, the system undergoes a *meandering* transition to the *diffusive* state, where transport of the microswimmers through the whole system occurs. The meandering transition depends on the obstacle density and the orbit radius as

$$n_m^*(\sigma/R) = n_c^* \frac{(\sigma/R)^2}{(\sigma/R + 1)^2}, \quad n_c^* = 0.359081\dots \quad (11)$$

This has been rationalized [54, 55] by an underlying percolation transition of disks made of obstacles and 'halos' thus associating an effective radius $\sigma + R$ to each obstacle. Last,

at densities $n^* > n_c^*$ a *localized* state emerges since the void space between the obstacles ceases to percolate, such that the microswimmers are trapped in separated pockets of void space, resulting in no long-range transport.

Here we explore the state diagram of our system and determine the diffusivity D for the noisy circle microswimmer in crowded environments. To illustrate our results we have computed contours of isodiffusivity, based on the data obtained from simulations. The linear system size $L = 10^4\sigma$ is such that finite size effects are irrelevant and computer simulation time is reasonable. The total simulation time is $10^5 - 10^7\sigma v_0^{-1}$. For each data point an average is performed over 200 – 400 disorder realization.

3. Results

First, we consider how adding rotational noise to the dynamics of an ideal microswimmer smears the meandering transition [6] and discuss the changes of the isodiffusivity lines. Next, we study the interplay of the two kinds of randomness, the dynamic angular noise and the quenched configurations of obstacles for different values of the orbit radius R . We highlight regions of the state diagram where diffusion is amplified and where it is suppressed.

3.1. State diagram and isodiffusivity contours

For any nonzero angular noise the meandering transition is smeared and the orbiting state is no longer present. Particles can reach different obstacle clusters by random reorientations, and this will always happen provided one waits long enough. The smearing of the phase transition is illustrated in Fig. 2(a,c) in terms of the diffusivity D as the density is increased towards the ideal meandering transition. The distance to the transition is characterized by a separation parameter $\varepsilon = (n^* - n_m^*(R))/n_m^*(R)$. Indeed, transport occurs now at any obstacle density due to the orientational noise. Yet, by lowering the angular noise D_θ the translational diffusion $D(R, D_\theta, n^*)$ approaches the case of the ideal microswimmer. Thus, the smearing of the transition is a continuous process and the results of the ideal microswimmer [6] remain valid for sufficiently small noise. The rate of convergence depends on the orbit radius. For small orbit radii [Fig. 2(a)] the convergence rate is slightly slower than for the larger ones [Fig. 2(c)]. This is due to the higher value of the obstacle density of the meandering transition for smaller orbit radii.

It should be mentioned that if translational diffusion was included, the meandering transition would also be smeared even in the absence of rotational noise. However, for realistic microswimmers the rotational diffusion is anticipated to be the main effect and the additional smearing due to translational diffusion should be small.

Now we zoom out from the meandering transition and consider the whole density range Fig. 2(b,d). For the intermediate obstacle densities the diffusivity D increases when the angular noise is increased up to its optimal value for a small orbit radius

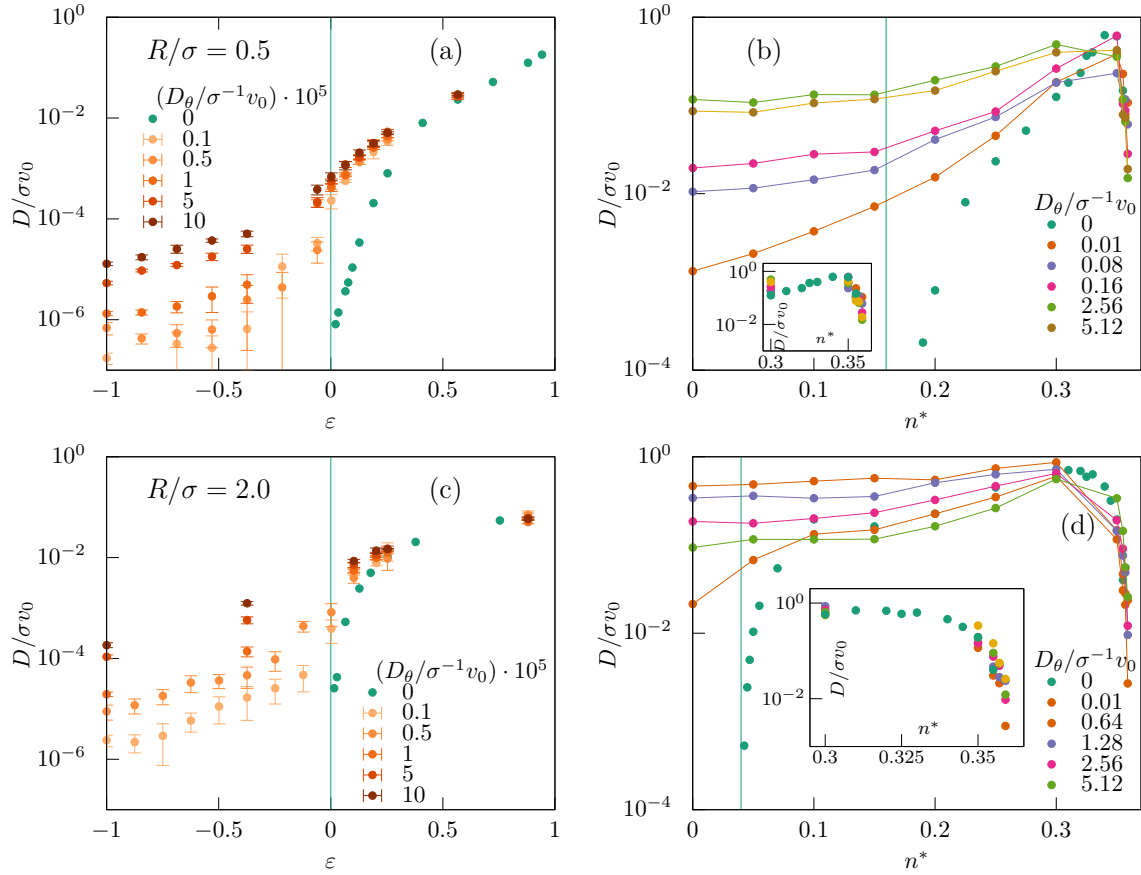


Figure 2. Diffusivity $D = D(R, D_\theta, n^*)$ vs. density of obstacles n^* (or separation parameter $\varepsilon = (n^* - n_m^*(R))/n_m^*(R)$) for orbit radius $R = 0.5\sigma$ (a,b) and $R = 2.0\sigma$ (c,d) for increasing values of the rotational diffusion D_θ . Vertical line shows the density $n_m^*(R)$ corresponding to the meandering transition, computed from Eq. (11). Panels (a) and (c) focus on the former *meandering* transition showing the data for small separation parameters ε and at relatively low angular noise. Panels (b) and (d) show the diffusivities over the full density range and at higher values of D_θ . Insets in panels (b,d) show close-ups of the diffusivity at high obstacle densities. Data for ideal microswimmer ($D_\theta = 0$) taken from Ref. [6].

Fig. 2(b) and a large one Fig. 2(c). At larger n^* , closer to the percolation transition, transport is dominated by the obstacles, in particular, by the crowding-enhancement transport mechanism, while angular noise is of minor importance. This can be seen in detail in the insets in Fig. 2(b,d). However, we note that the maximum diffusivity for each fixed curvature almost never exceeds the maximum value of the diffusivity in an ideal system, Fig. 2(b,d).

To get a more broad view we plot isodiffusivity contours in the state diagram spanned by the obstacle density n^* and the orbit curvature σ/R , as in the case of the ideal circle microswimmer [6] or the magneto-transport problem [55]. The diagrams are presented for increasing values of angular noise D_θ , see Fig. 3(a-d). In the second row, Fig. 3(e-h), the ratio of the diffusivity to its value for the idealized system ($D_\theta = 0$) is

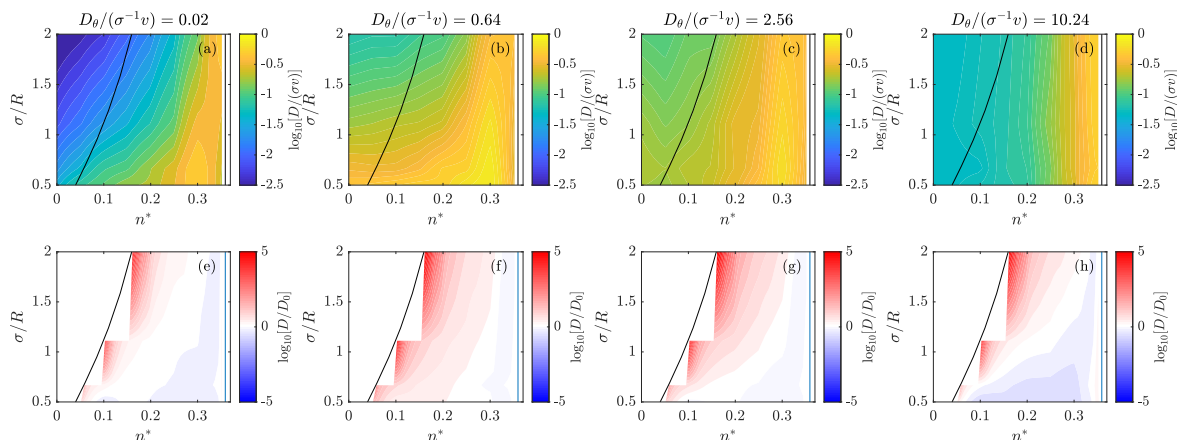


Figure 3. (a)-(d): Isodiffusivity contours $D = D(R, D_\theta, n^*)$, and (e)-(h): ratios of diffusivity to the diffusivity of the idealized model $D(R, D_\theta, n^*)/D(R, D_\theta = 0, n^*)$ in the state diagram spanned by obstacle density n^* and inverse orbit radius σ/R for increasing values of angular noise $D_\theta/\sigma^{-1}v_0$: (a),(e) 0.02, (b),(f) 0.64, (c),(g) 2.56, (d),(h) 10.24. In (a)-(d) color coding corresponds to $\log_{10}(D/\sigma v_0)$. In (e)-(h) red color corresponds to amplification whereas blue indicates suppression of diffusion. The black curve indicates the meandering transition of the ideal microswimmer model [6], Eq. (11). Note that to the left of the meandering transition for the ideal circle swimmer the diffusion coefficient evaluates to zero. The vertical black line shows the percolation transition at the density value $n_c^* = 0.359\dots$. In the panels of this figure, σ/R is used to facilitate the comparison with the ideal model, Ref. [6] and magneto-transport model, Ref. [55].

shown. For small noise D_θ , the diffusivity in the region above the meandering transition, $n^* > n_m^*(R)$ is very similar to the ideal case [Fig. 3(a)]. Only very close to the percolation transition there is a sharp drop of the diffusivity since swimmers become trapped in isolated pockets. In most of the parameter space corresponding to the diffusive state of the ideal circle swimmer, the values of the diffusivity D are again similar for both models. To the left of the meandering transition line, i.e. in the orbiting state, this ratio remains undefined [Fig. 3(e)]. Away from it, in most of the diffusive state, the light shading of the color coding indicates that the diffusivity there is very similar to the idealized case [Fig. 3(e)]. Approaching the meandering transition of the idealized model the diffusivity rapidly decreases, yet remains nonzero [Fig. 3(a)] in stark contrast to the idealized system where no diffusion in this region occurs.

For intermediate noise D_θ [Fig. 3(b,c)], the dependence of the diffusivity on the orbit radius is still strong even for the obstacle-free system $n^* = 0$, as suggested by Eq. (9). Upon increasing the density of obstacles the diffusivity again grows, however, the growth occurs mainly in the regime of the ideal diffusive state. For obstacle densities below the ideal meandering transition the dependence on the obstacle density is rather weak, such that the isodiffusivity lines are almost horizontal. An amplification of diffusion in the ideal diffusive state is revealed in Fig. 3(f,g).

For even higher angular noise [Fig. 3(d)] the dependence of the diffusivity on the

orbit radius fades out. This can be explained by the fact that the particle's free motion ceases to be circular, since the quality factor M is very low. Nevertheless, the diffusion coefficient increases with the density of obstacles except in the close vicinity of the percolation transition. In comparison to the ideal case, Fig. 3(h) shows that diffusion is suppressed in large areas of the parameter space.

The qualitative difference between the low and high noise behavior becomes immediately apparent upon inspecting typical trajectories, see Fig. 4. At low noise [Fig. 4(a)] the microswimmer trajectory in free space is composed of distorted circles, while for intermediate noise [Fig. 4(b)], the trajectories get significantly randomized and the noise promotes diffusion in free space.

In summary, low values of angular noise promote transport by allowing for the possibility to reach obstacle clusters which were inaccessible in the ideal case due to a limited orbit range. At intermediate noise values, the already efficient free-space transport is enhanced by the wall-following mechanism. At very large D_θ the circular motion is so rapidly randomized that transport approaches the case of an active Brownian tracer in a disordered environment, yet the wall-following mechanism enhances transport at high obstacle densities.

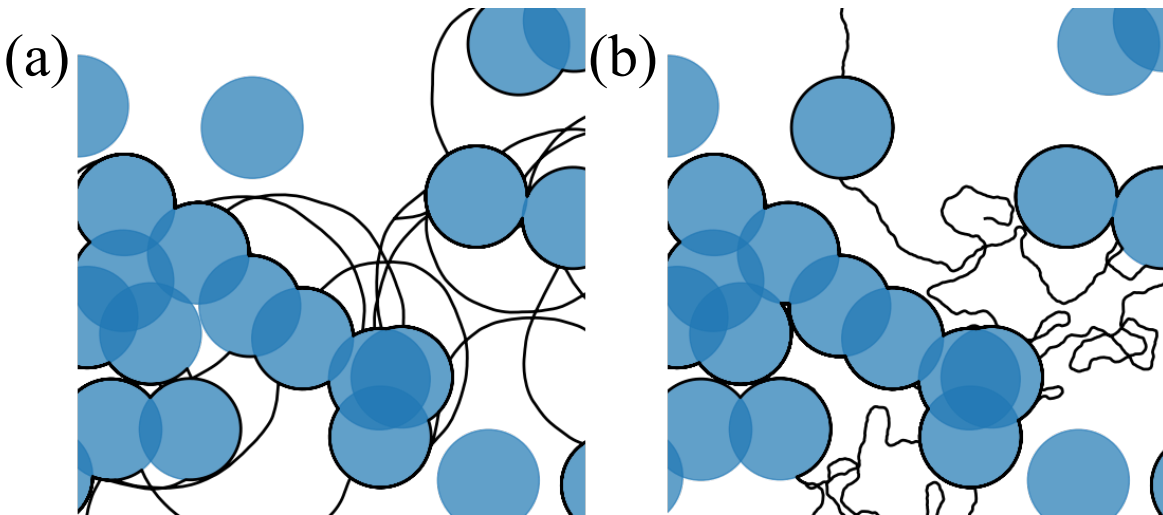


Figure 4. Trajectories of microswimmers (black) exploring the same array of obstacles (shown as blue circles) at obstacle density $n^* = 0.2$ (a) low noise, $D_\theta = 0.01\sigma^{-1}v_0$ and (b) intermediate noise, $D_\theta = 1.25\sigma^{-1}v_0$.

3.2. Amplification and suppression of transport

It is instructive to study directly the interplay of quenched disorder and dynamic noise. Therefore we redraw the isodiffusivity lines in a new state diagram spanned by the obstacle density n^* and the rotational diffusion coefficient D_θ for fixed orbit radius R , see Fig. 5(a-c). We highlight regions of amplification and suppression of diffusion by relating the computed contours to the diffusion coefficient at a small value of the

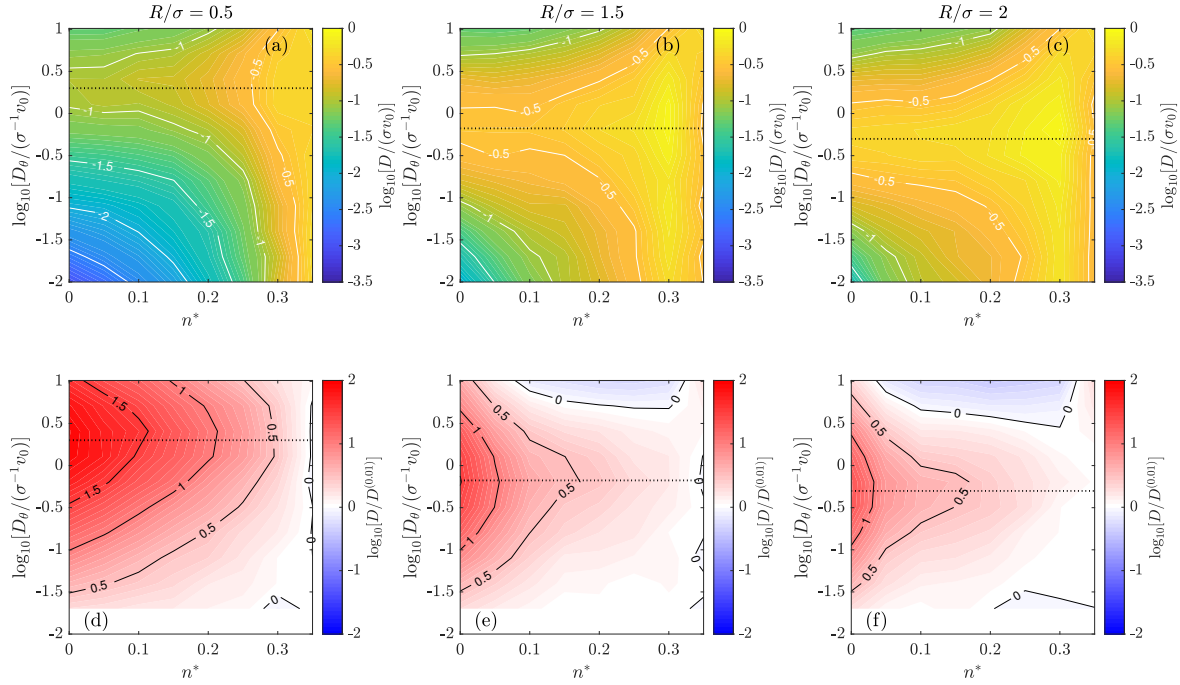


Figure 5. Panels (a,b,c) Isodiffusivity contours $D = D(R, D_\theta, n^*)$ in the plane $n^* - D_\theta$ for three orbit radii R/σ : (a,d) $R/\sigma = 0.5$, (b,e) $R/\sigma = 1.5$, (c,f) $R/\sigma = 2.0$. Color coding corresponds to $\log_{10} D/\sigma v_0$. Panels (d,e,f): $D/D^{(0.01)}$ Diffusion coefficient relative to the diffusion coefficient at a low value of the rotational noise, $D_\theta = 10^{-2}\sigma^{-1}v_0$. Red (blue) color corresponds to amplification (suppression) of diffusion. Dotted black lines correspond to the value of the rotational diffusion D_θ^{opt} which maximizes spatial diffusion D in the zero obstacle case, given by Eq. (10), and thus correspond to a quality factor value $M = 1/2\pi$.

rotational noise, Fig. 5(d-f). We choose a system with some rotational noise over the ideal system to have a more complete state diagram, without void regions of undefined value.

We can see that the diffusivity maps are qualitatively similar for three representative orbit radii, Fig. 5(a-c). The diffusivity continuously increases when the obstacle density is increased up to $n^* \simeq 0.3$. The line of constant angular noise $D_\theta = D_\theta^{\text{opt}}$ separates two regions. When the angular noise strength is increased up to the optimal value D_θ^{opt} , the diffusivity grows with it. However, as the angular noise is increased further the diffusivity starts to decrease for any value of the obstacle density. We note that for smaller radius [Fig. 5(a)] the optimal density of obstacles is very close to n_c^* , while for large radius [Fig. 5(b,c)] the optimal density value is closer to $n^* \approx 0.3$.

Next, we consider amplification or suppression of the diffusivity with respect to its value at low rotational noise

$$D^{(0.01)}(R, n^*) := D(R, D_\theta = 0.01 \sigma^{-1}v, n^*), \quad (12)$$

plotted in Fig. 5(d,e,f). In all three panels at $n^* = 0$ we see an enhancement of diffusion $D(D_\theta)/D^{(0.01)} > 1$ (indicated by the red color), which is solely due to the increase of angular noise, D_θ . When $n^* > 0$, an increase of rotational diffusion enhances the

diffusivity less and less for increasing density of obstacles. For the smallest radius $R = 0.5\sigma$, diffusion is almost always amplified [Fig. 5(d)]. For the intermediate radius $R = 1.5\sigma$, a region emerges at high obstacle densities where diffusion becomes suppressed when the angular noise is increased [Fig. 5(e)]. For the largest orbit radius $R = 2.0\sigma$, the size of this region increases [Fig. 5(f)]. From this we draw the conclusion that the area in parameter space covered by the suppression region increases with orbit radius.

While in general including angular noise and obstacles into the environment amplifies particle diffusion, for large values of both perturbations transport becomes hindered. The exact position of the boundary depends on the orbit radius R/σ , with smaller values of noise strength or obstacle density needed to cause a suppression of diffusion for larger radii.

4. Discussion.

4.1. Role of the Mean-Squared Displacement

In the *Results* section it has been elaborated that the amplification-suppression patterns are different for small ($R = 0.5\sigma$) [Fig. 5(d)] and large ($R = 1.5\sigma, 2.0\sigma$) radii [Fig. 5(e,f)]. For a small radius $R/\sigma = 0.5$ an amplification of transport with an increase of angular noise is observed at any obstacle density [Fig. 5(d)]. It qualitatively follows the diffusivity dependence on angular noise, given by the Eq. (9), where two values of angular noise, a low and high one, yield the same diffusivity value, causing similar amplification. However, for $R/\sigma = 2.0$ at intermediate-to-high densities the angular noise causes little amplification and even leads to suppression of diffusion at high noise values [Fig. 5(f)]. The long-time diffusivity given by Eq. (9) is not enough to explain this behavior.

To provide an intuitive explanation for such a drastic difference we consider the mean-squared displacement of an active circle Brownian swimmer in free space [48, 49, 53]

$$\begin{aligned} \delta r^2(t) = & \frac{2v_0^2 D_\theta^2}{(D_\theta^2 + \Omega^2)^2} \left[D_\theta t - 1 + \frac{\Omega^2}{D_\theta^2} (D_\theta t + 1) \right. \\ & \left. + \left(1 - \frac{\Omega^2}{D_\theta^2} \right) \cos(\Omega t) e^{-D_\theta t} - 2 \frac{\Omega}{D_\theta} \sin(\Omega t) e^{-D_\theta t} \right]. \end{aligned} \quad (13)$$

The mean-squared displacement typically evolves through three different regimes: directed motion (at short times), oscillations (at intermediate times), and diffusion (at long times). The duration of each of the regimes depends on the time scales Ω^{-1} and D_θ^{-1} .

To explain the difference in diffusivities at different D_θ for fixed n^* we consider the time needed to cover the characteristic distance between obstacles $\ell := \sigma/n^*$, termed the mean-free path length [56]. In some cases the particle can cover a distance ℓ already in the regime of directed motion (large R , large n^* , low D_θ). In other cases (high D_θ , low n^* , low R) the diffusive regime has been entered before the length ℓ is reached by

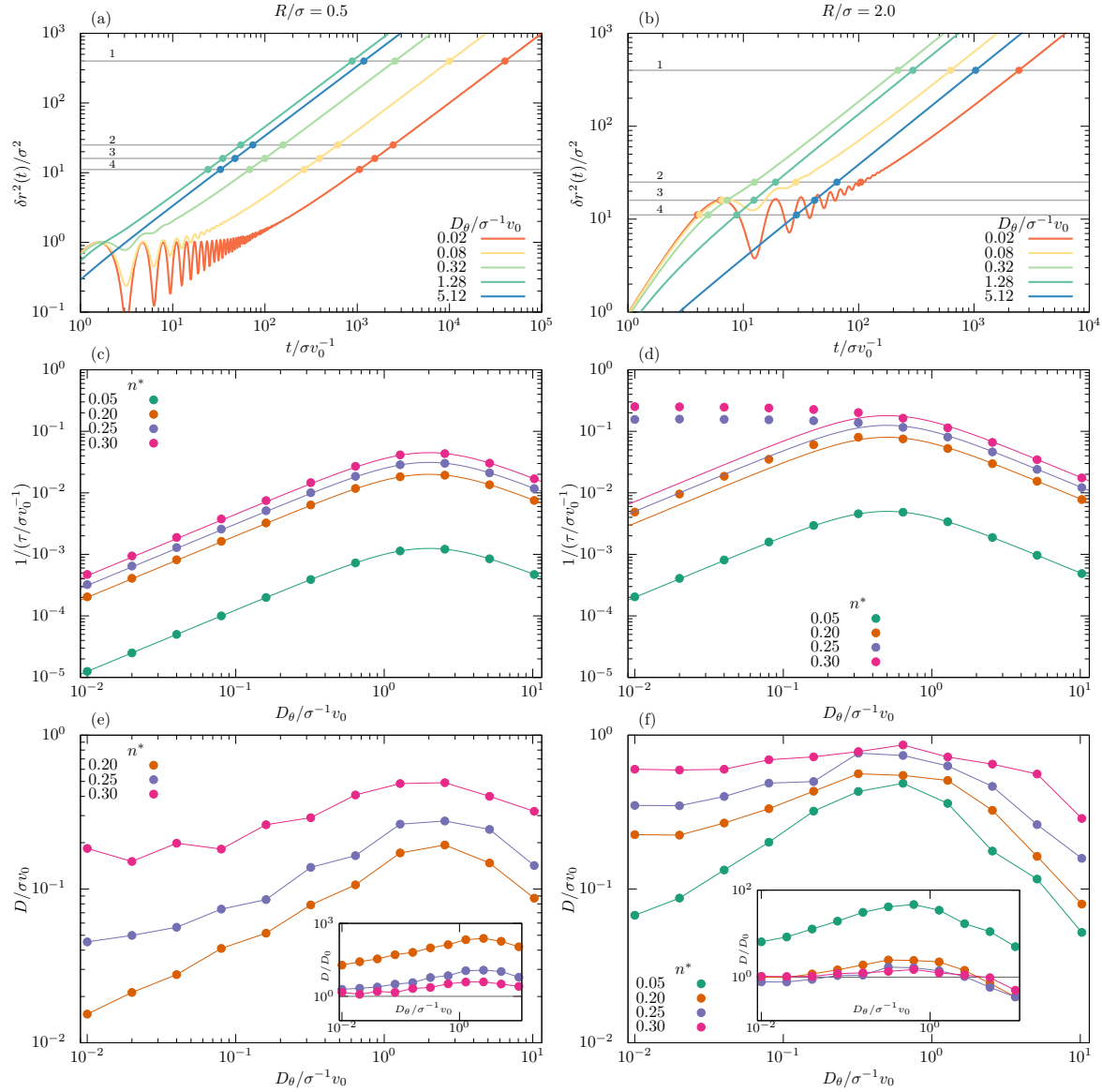


Figure 6. Mean-square displacements (curves) of a circle swimmer in an obstacle free environment for orbit radius $R = 0.5\sigma$ (a) and $R = 2.0\sigma$ (b) for different values of angular noise D_θ , plotted from Eq (13). Enumerated lines show the values of characteristic length squared ℓ^2 for different obstacle densities, (1) $\ell^2 = 400\sigma^2$, $n^* = 0.05$, (2) $\ell^2 = 25\sigma^2$, $n^* = 0.2$, (3) $\ell^2 = 16\sigma^2$, $n^* = 0.25$, (4) $\ell^2 = 11.1\dots\sigma^2$, $n^* = 0.3$. Points mark the characteristic time τ , obtained by graphical (numerical) solution. Inverse characteristic time $1/\tau$ as function of angular noise D_θ for $R = 0.5\sigma$ (c) and $R = 2.0\sigma$ (d) at several values of obstacle density n^* . Points represent graphical solutions, lines are given by Eq. (14). Diffusivity (main panels) and ratio of diffusivity to its ideal value at given density of obstacles $D(R, D_\theta, n^*)/D(R, D_\theta = 0, n^*)$ (insets) vs. angular noise D_θ , for $R = 0.5\sigma$ (e) and $R = 2.0\sigma$ (f). Lines in panels (e,f) serve as guides to the eye. Grey line in insets marks $D/D_0 = 1$.

the microswimmer. The difference can be quantified by a characteristic time τ , which can be directly inferred from the plot [Fig. 6(a,b)], as the first intersection of the mean-squared displacement curve with the line of constant ℓ^2 . For small radius ($R = 0.5\sigma$) the mean-squared displacements given by Eq. (13) display oscillations for low angular noise [Fig. 6(a)]. Their amplitude is small in comparison to the mean-free path ℓ for all obstacle densities considered, and the intersection always occurs in the diffusive regime. Thus, the time τ can be computed using the long-time asymptote for the mean-squared displacement, $\delta r^2(t) = 4Dt$, as $t \rightarrow \infty$, together with Eq. (9),

$$\tau = \frac{\ell^2}{2v_0^2 D_\theta} \left(D_\theta^2 + \frac{v_0^2}{R^2} \right). \quad (14)$$

In this case, Eq. (9) can be used to describe the variation in the diffusivity. In stark contrast, for large orbit radius ($R = 2.0$) [Fig. 6(b)] the microswimmer can access regions of distance ℓ while displaying circular motion. Thus, Eq. (9) alone is not enough to explain the results.

The inverse of the characteristic time τ is displayed in Fig. 6(c,d) as a function of D_θ . For $R = 0.5\sigma$, a non-monotonic behavior with a pronounced maximum for $1/\tau$ emerges at all densities [Fig. 6(c)], according to Eq. (14). Yet, for $R = 2.0\sigma$ beyond a density $n^* \gtrsim 0.25$ the dependence becomes monotonically decreasing [Fig. 6(d)] and solutions of the full equation (graphical solutions) deviate from the approximation, Eq. (14), at low values of D_θ . In both cases the dependence of the diffusivity D on the angular noise D_θ correlates with $1/\tau$. For $R = 0.5\sigma$ the result is not surprising, as D vs. D_θ is also a non-monotonic function with the maximum at the corresponding position [Fig. 6(e)]. From the idealized model we know that a higher obstacle density provides a larger diffusion [6], thus the amplitude of the amplification decreases with n^* . Most importantly, the diffusivity never becomes suppressed [Fig. 6(e) inset].

For large radius $R = 2.0\sigma$ the argument is more subtle [Fig. 6(f)]. At low densities, $n^* \approx 0.05$, the behavior is the same as for small radius. For high densities $n^* \gtrsim 0.2$ the diffusivity remains almost constant (similar to its value of the idealized model) as the noise is increased. It becomes slightly amplified around the optimal noise value D_θ^{opt} , and for D_θ larger than D_θ^{opt} the diffusion is suppressed. Considering the diffusivity ratios [Fig. 6(f) inset] only the low-density $n^* = 0.05$ is similar to the $R = 0.5$ case [Fig. 6(e) inset]. All other curves do not quite follow the $1/\tau$ curves at low noises. While the characteristic time to cover ℓ^2 only increases with D_θ [Fig. 6(d)], the diffusivity D nevertheless is amplified around the optimal angular noise D_θ^{opt} [Fig. 6(f) inset]. For larger values of angular noise the $1/\tau$ and D curves decrease in a correlated way [Fig. 6(d) and (f) inset]. So, the characteristic time τ is no longer sufficient, rather we anticipate that the entire distribution of times needed to cover an entire range of path lengths slightly larger than ℓ determines the transport properties.

For an ideal microswimmer the time τ to cover an arbitrary distance λ increases until the length scale becomes equal to the orbit diameter, $\lambda = 2R$. For larger values of $\lambda > 2R$ the characteristic time τ does not exist, as the ideal microswimmer cannot travel farther than $2R$. If a small amount of angular noise is introduced, length

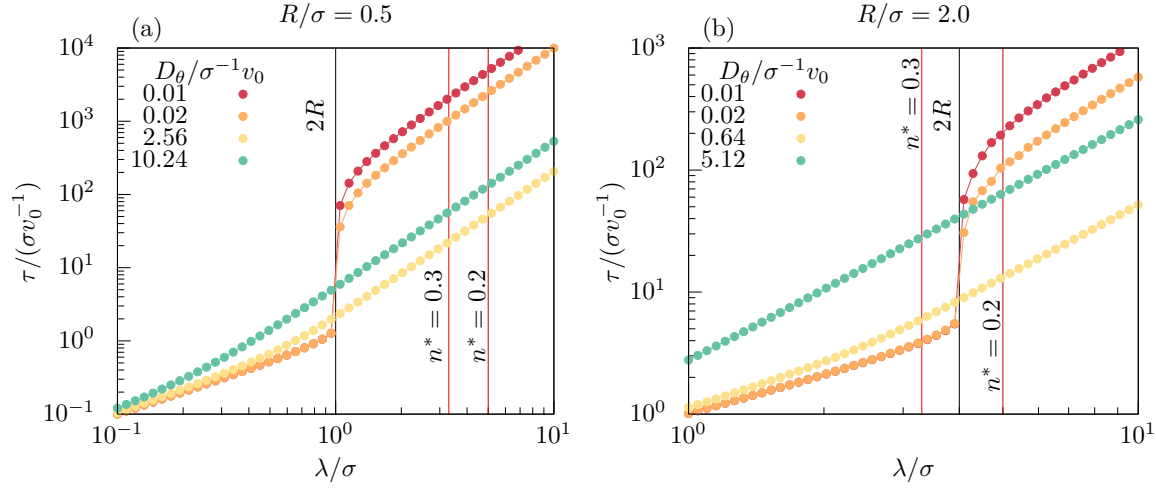


Figure 7. Characteristic time τ vs. distance λ for various values of the angular noise D_θ for (a) $R/\sigma = 0.5$ ($D_\theta^{\text{opt}} = 2.0\sigma^{-1}v_0$) and (b) $R/\sigma = 2.0$ ($D_\theta^{\text{opt}} = 0.5\sigma^{-1}v_0$). Black lines indicate the diameter $2R$ and the two red lines show the characteristic lengths corresponding to obstacle density $n^* = 0.20$ and $n^* = 0.30$.

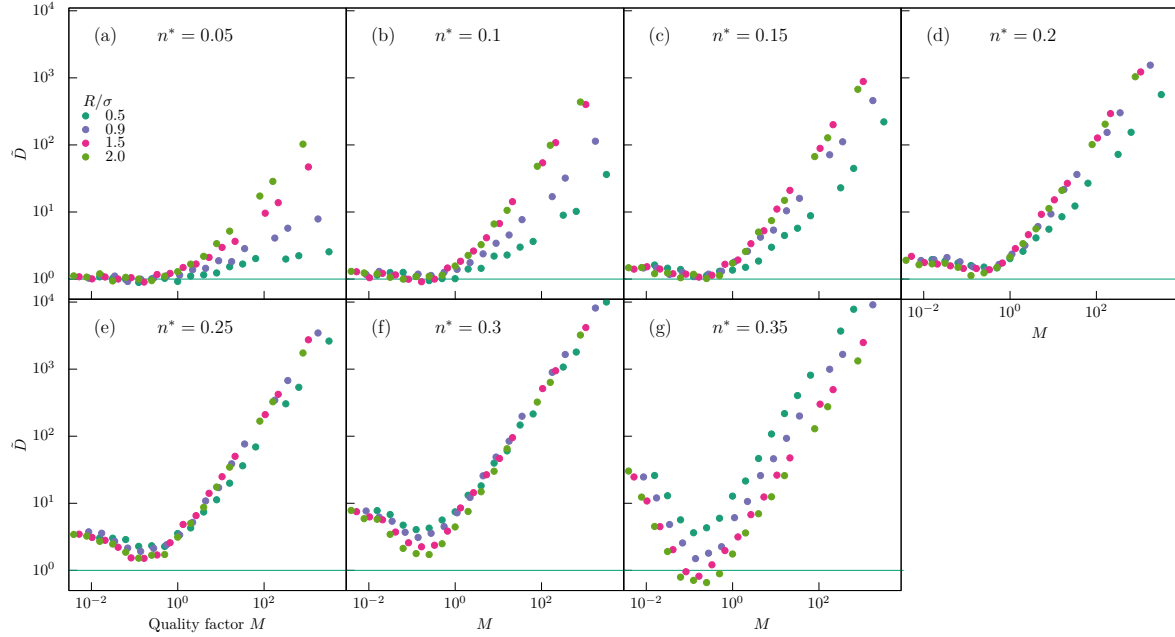


Figure 8. Rescaled diffusivity $\tilde{D} = \tilde{D}(R, M, n^*)$ [Eq. (15)] as a function of quality factor M . Panels (a)-(g) show the dependence for increasing obstacle densities n^* . Different colors represent different values of the orbit radius. In each panel the green line indicates 1, which is the rescaled diffusivity in the absence of obstacles.

scales $\lambda > 2R$ become accessible, but the time to cover them is significantly larger compared to the time to cover $\lambda = 2R$. The dependence of τ on an arbitrary length scale λ is rather steep at low noise values in the vicinity of $\lambda \approx 2R$, see Fig. 7. For $R = 0.5\sigma$ this step increase occurs far away from the characteristic lengths defined by

the largest considered densities [Fig. 7 (a)], and thus has no impact on the amplification-suppression pattern. For $R = 2.0\sigma$ the values of $\ell(n^*)$ at $n^* \gtrsim 0.2$ are comparable with the diameter $2R$, for example, $\ell(n^* = 0.25) = 2R = 4\sigma$, [Fig. 7(b)]. The amplification of diffusion at low noises ($D_\theta \ll D_\theta^{\text{opt}}$) is absent because the characteristic times to cover small distances are comparable with the ones for the ideal system $\tau(\lambda < 2R, D_\theta \ll 1) \approx \tau(\lambda < 2R, D_\theta = 0)$. Yet, times to cover slightly farther distances are quite large $\tau(\lambda > 2R, D_\theta \ll D_\theta^{\text{opt}}) \gg \tau(\lambda < 2R, D_\theta \ll D_\theta^{\text{opt}})$ and do not affect the transport properties [Fig. 7(b), red and orange curves]. If the angular noise is increased up to its optimal value, $D_\theta \approx D_\theta^{\text{opt}}$, the time to cover small distances also increases, $\tau(\lambda < 2R, D_\theta \approx D_\theta^{\text{opt}}) > \tau(\lambda < 2R, D_\theta = 0)$ [Fig. 7(b), yellow curve]. However, the time to cover larger distances decreases drastically and the steep increase becomes smooth. The latter effect is more important and an amplification of transport is observed. With a further increase of angular noise beyond its optimal value all characteristic times also increase, both for small $\lambda < 2R$ and large $\lambda > 2R$ length scales [Fig. 7(b), aquamarine curve]. Hence, transport becomes suppressed. This picture holds for obstacle densities below $n^* = 0.3$ while the average length scale ℓ remains comparable to $2R$. As soon as the density becomes too low, for example $n^* = 0.05$, the simple mechanism described for $R = 0.5$ is valid.

4.2. Quality factor M as a bridge to possible experimental results.

So far we have presented our study from the perspective of increasing the angular noise strength at a constant density of obstacles. However, in an experimental setup such a strategy might be not possible. While in experiments it is difficult to control the rotational diffusion coefficient, the obstacle density may be varied. For a direct comparison with experimentally accessible control parameters we represent the data in terms of two dimensionless quantities, the quality factor M and the ratio of diffusion in a crowded system to the diffusion in an obstacle-free system. We show how the diffusivity is amplified or suppressed at different obstacle densities for a range of quality factors. We discuss $D = D(R, M, n^*)$ as a function of the quality factor M with fixed orbit radius and obstacle density, rather than as a function of the (reduced) orientational diffusivity. Therefore we define the rescaled diffusivity

$$\tilde{D} = \tilde{D}(R, M, n^*) := D(R, M, n^*)/D(R, M, n^* = 0), \quad (15)$$

which by construction reduces at zero obstacle density to $\tilde{D}(R, M, n^* = 0) = 1$. Indeed, from the simulations we see that for low obstacle density $\tilde{D} \approx 1$ holds for quality factors below the optimal one, $M \lesssim M^{\text{opt}} = 1/2\pi$ [Fig. 8(a,b)]. At these low densities, increasing the quality factor beyond the optimal one leads to an increase of the rescaled diffusivity. Moreover, a larger amplification is observed for a larger R/σ ratio. This observation suggests that scattering at an isolated obstacle is more efficient in accelerating transport if the orbit radius is larger than the obstacle size. Propagation around the boundary of a small obstacle cluster, or even a single obstacle, facilitates

meandering thus increasing the diffusivity. This effect becomes more pronounced for larger radii.

For somewhat larger densities, the diffusivity shows a minimum at the optimal quality factor value [Fig. 8(c-f)]. This occurs together with another striking observation: for densities $n^* \lesssim 0.25 - 0.30$ there is an approximate data collapse for different radii R [Fig. 8(e,f)]. This feature is a peculiarity for microswimmers and is connected to the wall-following mechanism. We have checked that for specular scattering off the obstacles as in magneto-transport this data collapse does not occur.

In the case of the highest density $n^* = 0.35$ close to the percolation transition n_c^* there is still a pronounced minimum in the amplification at $M = M^{\text{opt}}$ [Fig. 8(g)], yet the dependence on the orbit radius becomes significant. In the ideal model at obstacle densities around $n^* = 0.35$ the disordered structure ceases to amplify transport and starts to suppress it, as at n_c^* one expects the diffusivity to become zero. At this density the pockets of the void space appear connected by narrow channels. From the data one can conclude that particles with smaller orbit radii are more efficient in moving through such a structure than their counterparts with larger orbit radii. Then the order of the curves at high density [Fig. 8(g)] is reversed in comparison to the low density $n^* = 0.05$, [Fig. 8(a)]. The same effect has been reported for ideal microswimmers where it was also seen that the diffusivity at very high obstacle densities is larger for smaller orbit radii [6], compare aquamarine points in Fig. 2(b) $R = 0.5\sigma$ and (d) $R = 2.0\sigma$.

To summarize this part, we find that at all densities the shape of the amplification curve remains the same. At low M there is no to little amplification. At M^{opt} the amplification is minimal, but then quickly increases for larger values of M .

The properties described above can serve as a guideline for future experiments. The quality factor of the orbit can be easily identified for the given experimental probe particle (biological or artificial) and then one can verify the prediction for the amplification curves at different obstacle densities. The best correspondence between experiment and theory is expected for particles that are well described by our model. This is those that become trapped around obstacles and can travel large distances before departing from the obstacle boundary.

5. Summary and Conclusions

We have investigated the transport properties of a noisy circular microswimmer exploring a heterogeneous environment that consists of overlapping non-permeable obstacles. We have employed a boundary-following mechanism accounting for the microswimmer's specific interactions with obstacles. These interactions are distinct from non-motile particles which instead exhibit specular reflection. For our microswimmers, a small noise and a low spatial disorder lead to an enhancement of transport and to an overall increase of the diffusivity. Adding angular noise to an ideal circle microswimmer allows the active particle to meander from one cluster of overlapping obstacles to another faster and more efficiently. Additionally, by increasing the obstacle density

an amplification of transport is achieved, since obstacles promote propagation in a swift way along their edges. However, a further increase of randomness, by the addition of more angular noise strongly suppresses transport again, in particular for large orbit radii.

As our main finding we have identified that the time to cover a characteristic inter-obstacle distance is the main parameter that governs the amplification-suppression patterns. We have shown that at small radii the microswimmers with noise can propagate efficiently in a diffusive regime. However, for larger radii the diffusive regime causes the transport suppression.

To identify which effects are purely the consequences of the introduced wall-following mechanism we have performed numerical simulations of a corresponding model but with specular reflections from the obstacles. Such a model is relevant for magneto-transport of electrons in disordered environments where noise due to scattering from phonons becomes relevant. For such specular scattering the diffusivity is non-monotonic in the obstacle density with a pronounced maximum [55, 57] at an intermediate value far from n_c^* . If the noise is increased, the maximum of the diffusivity is systematically shifted to even lower obstacle densities, thus at high densities the diffusivity becomes suppressed in strong contrast to the wall-following mechanism.

To relate our model to experiments, more details on the interaction mechanism with the obstacles should be taken into account. For example, as a first step one can let the direction of motion evolve by a noisy dynamics while the swimmer interacts with the obstacle. Moreover, the explicit equation for the swimmer interaction with an obstacle could be taken from Ref. [31] to substitute the rule in the current paper. These will serve as important steps in further modeling of the microswimmer dynamics in crowded media. We expect the main findings to remain the same, but a better correspondence with experiments could be achieved.

Insight can be taken from recent biological experiments. For example, *E. Coli* bacteria do not just follow the boundaries, but can experience specular scattering events depending on the angle of approach to the obstacle [5]. Their diffusivity increases if a small number of obstacles is added, but decreases upon further increase of the obstacle density. This is in qualitative agreement with our results.

If the translational diffusion is non-zero the meandering transition will be smeared even for vanishing rotational diffusion. Correspondingly, one anticipates parameter regimes (for particles closer to passive ones) such that translational diffusion yields the main contribution to the smearing, rather than orientational diffusion. An interesting extension of our work would be to elaborate the competition between both stochastic noises.

It is also interesting to generalize to visco-elastic media [17, 18], as many microorganisms move in non-Newtonian biological fluids [58, 59]. This can be achieved in principle by changing the dynamic rules of motion in the void space, as well as the particle-obstacle interaction. Another extension of the model is to consider driven systems [14, 60, 61, 62] where external driving forces, flows, or chemical gradients

are present. This extension is important, as experiments on motile bacteria transport through porous media are typically performed in microfluidic devices with an imposed flow [35].

A natural extension of our model is to consider interacting active circle swimmers in the presence of obstacles. For the passive counterpart recent simulations [63] have revealed a striking speed-up of transport, while in bulk interacting particles typically slow down transport and may lead to structural arrest. Active circle swimmers at low densities may similarly promote transport since they will push each other to the walls where the wall-following mechanism sets in. In contrast at high swimmer densities they may get trapped or jammed at the boundaries of the obstacles, such that the wall-following mechanism is no longer efficient.

For future applications one may ask if an agent can adjust its motility parameters depending on its local environment. In state-of-the-art experiments [64, 65] a direct control of the active particles can be achieved to mimic such a behavior. In the future active agents may be designed that display a dynamic feedback to optimize locally their transport in a given landscape of obstacles. A step even further are smart agents that can design their own rules to achieve common goals which have been discussed only recently [66, 67].

Acknowledgements

We thank Felix Höfling for insightful discussions. We thank Charlotte Petersen for discussions and careful reading of the final version of the manuscript. OC is supported by the Austrian Science Fund (FWF): M 2450-NBL. TF acknowledges funding by FWF: P 28687-N27. The computational results presented have been achieved in part using the HPC infrastructure LEO of the University of Innsbruck.

References

- [1] Romanczuk P, Bär M, Ebeling W, Lindner B and Schimansky-Geier L 2012 *The European Physical Journal Special Topics* **202** 1–162 ISSN 1951-6401 URL <http://dx.doi.org/10.1140/epjst/e2012-01529-y>
- [2] Elgeti J, Winkler R G and Gompper G 2015 *Reports on Progress in Physics* **78** 056601 URL <http://stacks.iop.org/0034-4885/78/i=5/a=056601>
- [3] Bechinger C, Di Leonardo R, Löwen H, Reichhardt C, Volpe G and Volpe G 2016 *Rev. Mod. Phys.* **88**(4) 045006 URL <https://link.aps.org/doi/10.1103/RevModPhys.88.045006>
- [4] Reichhardt C O and Reichhardt C 2017 *Annual Review of Condensed Matter Physics* **8** 51–75 URL <https://doi.org/10.1146/annurev-conmatphys-031016-025522>
- [5] Makarchuk S, Braz V C, Araújo N A M, Ciric L and Volpe G 2019 *Nature Communications* **10** 4110 ISSN 2041-1723 URL <https://doi.org/10.1038/s41467-019-12010-1>
- [6] Chepizhko O and Franosch T 2019 *Soft Matter* **15**(3) 452–461 URL <http://dx.doi.org/10.1039/C8SM02030B>
- [7] Jakuszeit T, Croze O A and Bell S 2019 *Phys. Rev. E* **99**(1) 012610 URL <https://link.aps.org/doi/10.1103/PhysRevE.99.012610>

- [8] Chepizhko O and Peruani F 2013 *Phys. Rev. Lett.* **111**(16) 160604 URL <http://link.aps.org/doi/10.1103/PhysRevLett.111.160604>
- [9] Zeitz M, Wolff K and Stark H 2017 *The European Physical Journal E* **40** 23 ISSN 1292-895X URL <http://dx.doi.org/10.1140/epje/i2017-11510-0>
- [10] Morin A, Lopes Cardozo D, Chikkadi V and Bartolo D 2017 *Phys. Rev. E* **96**(4) 042611 URL <https://link.aps.org/doi/10.1103/PhysRevE.96.042611>
- [11] Sosa-Hernández J E, Santillán M and Santana-Solano J 2017 *Phys. Rev. E* **95**(3) 032404 URL <https://link.aps.org/doi/10.1103/PhysRevE.95.032404>
- [12] Frangipane G, Vizsnyiczai G, Maggi C, Savo R, Sciortino A, Gigan S and Di Leonardo R 2019 *Nature Communications* **10** 2442 ISSN 2041-1723 URL <https://doi.org/10.1038/s41467-019-10455-y>
- [13] Bénichou O, Illien P, Oshanin G, Sarracino A and Voituriez R 2014 *Phys. Rev. Lett.* **113**(26) 268002 URL <https://link.aps.org/doi/10.1103/PhysRevLett.113.268002>
- [14] Reichhardt C and Reichhardt C J O 2018 *Journal of Physics: Condensed Matter* **30** 015404 URL <http://stacks.iop.org/0953-8984/30/i=1/a=015404>
- [15] Bénichou O, Illien P, Oshanin G, Sarracino A and Voituriez R 2018 *Journal of Physics: Condensed Matter* **30** 443001 URL <http://stacks.iop.org/0953-8984/30/i=44/a=443001>
- [16] Péter H, Libál A, Reichhardt C and Reichhardt C J O 2018 *Scientific Reports* **8** 10252 ISSN 2045-2322 URL <https://doi.org/10.1038/s41598-018-28256-6>
- [17] Lozano C, Gomez-Solano J R and Bechinger C 2018 *New Journal of Physics* **20** 015008 URL <https://doi.org/10.1088/1367-2630/aa9ed1>
- [18] Narinder N, Bechinger C and Gomez-Solano J R 2018 *Phys. Rev. Lett.* **121**(7) 078003 URL <https://link.aps.org/doi/10.1103/PhysRevLett.121.078003>
- [19] ten Hagen B, Kümmel F, Wittkowski R, Takagi D, Löwen H and Bechinger C 2014 *Nature Communications* **5** 4829 article URL <http://dx.doi.org/10.1038/ncomms5829>
- [20] Friedrich B M and Jülicher F 2008 *New Journal of Physics* **10** 123025 URL <http://stacks.iop.org/1367-2630/10/i=12/a=123025>
- [21] Kaupp U B and Alvarez L 2016 *The European Physical Journal Special Topics* **225** 2119–2139 ISSN 1951-6401 URL <https://doi.org/10.1140/epjst/e2016-60097-1>
- [22] Brun-Cosme-Bruny M, Bertin E, Coasne B, Peyla P and Rafaï S 2019 *The Journal of Chemical Physics* **150** 104901 (Preprint <https://doi.org/10.1063/1.5081507>) URL <https://doi.org/10.1063/1.5081507>
- [23] Reichhardt C and Reichhardt C J O 2013 *Phys. Rev. E* **88**(4) 042306 URL <https://link.aps.org/doi/10.1103/PhysRevE.88.042306>
- [24] Denissenko P, Kantsler V, Smith D J and Kirkman-Brown J 2012 *Proceedings of the National Academy of Sciences* **109** 8007–8010 URL <https://doi.org/10.1073/pnas.1202934109>
- [25] Takagi D, Palacci J, Braunschweig A B, Shelley M J and Zhang J 2014 *Soft Matter* **10**(11) 1784–1789 URL <http://dx.doi.org/10.1039/C3SM52815D>
- [26] Nosrati R, Driouchi A, Yip C M and Sinton D 2015 *Nature Communications* **6** 8703
- [27] Brown A T, Vladescu I D, Dawson A, Vissers T, Schwarz-Linek J, Lintuvuori J S and Poon W C K 2016 *Soft Matter* **12**(1) 131–140 URL <http://dx.doi.org/10.1039/C5SM01831E>
- [28] Davies Wykes M S, Zhong X, Tong J, Adachi T, Liu Y, Ristroph L, Ward M D, Shelley M J and Zhang J 2017 *Soft Matter* **13**(27) 4681–4688 URL <http://dx.doi.org/10.1039/C7SM00203C>
- [29] Lauga E, DiLuzio W R, Whitesides G M and Stone H A 2006 *Biophysical Journal* **90** 400–412 ISSN 0006-3495 URL <http://dx.doi.org/10.1529/biophysj.105.06940>
- [30] Berke A P, Turner L, Berg H C and Lauga E 2008 *Phys. Rev. Lett.* **101**(3) 038102 URL <http://link.aps.org/doi/10.1103/PhysRevLett.101.038102>
- [31] Spagnolie S E, Moreno-Flores G R, Bartolo D and Lauga E 2015 *Soft Matter* **11**(17) 3396–3411 URL <http://dx.doi.org/10.1039/C4SM02785J>
- [32] Kuron M, Stärk P, Holm C and de Graaf J 2019 *Soft Matter* Advance Article URL <http://dx.doi.org/10.1039/C9SM00692C>

- [33] Bertrand T, Zhao Y, Bénichou O, Tailleur J and Voituriez R 2018 *Phys. Rev. Lett.* **120**(19) 198103 URL <https://link.aps.org/doi/10.1103/PhysRevLett.120.198103>
- [34] Kamal A and Keaveny E E 2018 *Journal of The Royal Society Interface* **15** 20180592 URL <https://doi.org/10.1098/rsif.2018.0592>
- [35] Creppy A, Clément E, Douarche C, D'Angelo M V and Auradou H 2019 *Phys. Rev. Fluids* **4**(1) 013102 URL <https://link.aps.org/doi/10.1103/PhysRevFluids.4.013102>
- [36] Chamolly A, Ishikawa T and Lauga E 2017 *New Journal of Physics* **19** 115001 URL <http://stacks.iop.org/1367-2630/19/i=11/a=115001>
- [37] Sándor C, Libál A, Reichhardt C and Reichhardt C J O 2017 *Phys. Rev. E* **95**(1) 012607 URL <https://link.aps.org/doi/10.1103/PhysRevE.95.012607>
- [38] Lorentz H A 1905 *Arch. Neerl. Sci. Exactes Nat.* **10** –
- [39] Bauer T, Höfling F, Munk T, Frey E and Franosch T 2010 *The European Physical Journal Special Topics* **189** 103–118 ISSN 1951-6401 URL <https://doi.org/10.1140/epjst/e2010-01313-1>
- [40] Mandal S, Spanner-Denzer M, Leitmann S and Franosch T 2017 *The European Physical Journal Special Topics* **226** 3129–3156 ISSN 1951-6401 URL <https://doi.org/10.1140/epjst/e2017-70077-5>
- [41] Schnyder S K, Spanner M, Höfling F, Franosch T and Horbach J 2015 *Soft Matter* **11**(4) 701–711 URL <http://dx.doi.org/10.1039/C4SM02334J>
- [42] Spanner M, Schnyder S K, Höfling F, Voigtmann Th and Franosch T 2013 *Soft Matter* **9**(5) 1604–1611 URL <http://dx.doi.org/10.1039/C2SM27060A>
- [43] Höfling F and Franosch T 2013 *Reports on Progress in Physics* **76** 046602 URL <http://stacks.iop.org/0034-4885/76/i=4/a=046602>
- [44] Petersen C F and Franosch T 2019 *Soft Matter* **15**(19) 3906–3913 URL <http://dx.doi.org/10.1039/C9SM00442D>
- [45] Kümmel F, ten Hagen B, Wittkowski R, Buttinoni I, Eichhorn R, Volpe G, Löwen H and Bechinger C 2013 *Phys. Rev. Lett.* **110**(19) 198302 URL <http://link.aps.org/doi/10.1103/PhysRevLett.110.198302>
- [46] Utada A S, Bennett R R, Fong J C N, Gibiansky M L, Yildiz F H, Golestanian R and Wong G C L 2014 *Nature Communications* **5** 4913 article URL <http://dx.doi.org/10.1038/ncomms5913>
- [47] Ipiña E P, Otte S, Pontier-Bres R, Czerucka D and Peruani F 2019 *Nature Physics* **15** 610–615 URL <https://doi.org/10.1038/s41567-019-0460-5>
- [48] van Teeffelen S and Löwen H 2008 *Phys. Rev. E* **78**(2) 020101 URL <https://link.aps.org/doi/10.1103/PhysRevE.78.020101>
- [49] Kurzthaler C and Franosch T 2017 *Soft Matter* **13**(37) 6396–6406 URL <http://dx.doi.org/10.1039/C7SM00873B>
- [50] Basu U, Majumdar S N, Rosso A and Schehr G 2019 *Physical Review E* **100** URL <https://doi.org/10.1103/physreve.100.062116>
- [51] Scala A, Voigtmann Th and De Michele C 2007 *The Journal of Chemical Physics* **126** 134109 (Preprint <https://doi.org/10.1063/1.2719190>) URL <https://doi.org/10.1063/1.2719190>
- [52] Höfling F, Franosch T and Frey E 2006 *Phys. Rev. Lett.* **96**(16) 165901 URL <https://link.aps.org/doi/10.1103/PhysRevLett.96.165901>
- [53] Ebbens S, Jones R A L, Ryan A J, Golestanian R and Howse J R 2010 *Phys. Rev. E* **82**(1) 015304 URL <https://link.aps.org/doi/10.1103/PhysRevE.82.015304>
- [54] Kuzmany A and Spohn H 1998 *Phys. Rev. E* **57**(5) 5544–5553 URL <https://link.aps.org/doi/10.1103/PhysRevE.57.5544>
- [55] Schirmacher W, Fuchs B, Höfling F and Franosch T 2015 *Phys. Rev. Lett.* **115**(24) 240602 URL <http://link.aps.org/doi/10.1103/PhysRevLett.115.240602>
- [56] Franosch T, Höfling F, Bauer T and Frey E 2010 *Chemical Physics* **375** 540 – 547 URL <http://www.sciencedirect.com/science/article/pii/S0301010410001898>
- [57] Siboni N H, Schluck J, Pierz K, Schumacher H W, Kazazis D, Hor-

- bach J and Heinzl T 2018 *Phys. Rev. Lett.* **120**(5) 056601 URL <https://link.aps.org/doi/10.1103/PhysRevLett.120.056601>
- [58] Martinez V A, Schwarz-Linek J, Reufer M, Wilson L G, Morozov A N and Poon W C K 2014 *Proceedings of the National Academy of Sciences* **111** 17771–17776 ISSN 0027-8424 (*Preprint* <https://www.pnas.org/content/111/50/17771.full.pdf>) URL <https://www.pnas.org/content/111/50/17771>
- [59] Zöttl A and Yeomans J M 2019 *Nature Physics* **15** 554–558 URL <https://doi.org/10.1038/s41567-019-0454-3>
- [60] Leitmann S and Franosch T 2013 *Phys. Rev. Lett.* **111**(19) 190603 URL <https://link.aps.org/doi/10.1103/PhysRevLett.111.190603>
- [61] Reichhardt C and Olson Reichhardt C J 2014 *Phys. Rev. E* **90**(1) 012701 URL <https://link.aps.org/doi/10.1103/PhysRevE.90.012701>
- [62] Reichhardt C and Reichhardt C J O 2019 *Phys. Rev. E* **100**(1) 012604 URL <https://link.aps.org/doi/10.1103/PhysRevE.100.012604>
- [63] Schnyder S K and Horbach J 2018 *Physical Review Letters* **120** URL <https://doi.org/10.1103/physrevlett.120.078001>
- [64] Lavergne F A, Wendehenne H, Bäuerle T and Bechinger C 2019 *Science* **364** 70–74 URL <https://doi.org/10.1126/science.aau5347>
- [65] Fernandez-Rodriguez M A, Grillo F, Alvarez L, Rathlef M, Buttinoni I, Volpe G and Isa L 2019 Active colloids with position-dependent rotational diffusivity (*Preprint* [arXiv:1911.02291](https://arxiv.org/abs/1911.02291))
- [66] Ried K, Müller T and Briegel H J 2019 *PLOS ONE* **14** e0212044 URL <https://doi.org/10.1371/journal.pone.0212044>
- [67] Charlesworth H J and Turner M S 2019 *Proceedings of the National Academy of Sciences* **116** 15362–15367 URL <https://doi.org/10.1073/pnas.1822069116>